Available online at www.sciencedirect.com
ScienceDirect
International Journal of Heat and Mass Transfer 50 (2007) 4275–4285
International Journal of HEAT and MASS TRANSFER
www.elsevier.com/locate/ijhmt

Effects of water and *iso*-propyl alcohol relative humidities on single wafer cleaning system performance

J. Koo [a,*], T. Kim [a], C. Jung [a], J. Lee [a], T. Kim [b]

[a] *Samsung Advanced Institute of Technology, Mt. 14-1, Nongseo-dong, Giheung-gu, Yongin-si, Gyunggi-do 449-712, South Korea*
[b] *Samsung Electronics, Mt. 24, Nongseo-dong, Giheung-gu, Yongin-si, Gyunggi-do 449-711, South Korea*

Received 18 July 2006; received in revised form 10 January 2007
Available online 7 June 2007

Abstract

As the pattern size scales down and the wafer size increases, the particle defects should be controlled more strictly in the modern microelectronics fabrication. Single wafer cleaning processes are introduced in the industry due to higher particle removal efficiency and lower particle reattachment possibility. In this study, the origins of watermark defects in single wafer cleaning system were identified, and the ways to avoid the problems were suggested through a model based numerical simulation. The watermark defects observed in the single wafer cleaning systems were found to originate from the failure of controlling water and *iso*-propyl alcohol (IPA) relative humidities in the surrounding gas. Increasing the IPA relative humidity in the surrounding gas during the drying phase could improve watermark defects and increase product yields.

Keywords: Single wafer cleaning; Relative humidity; Evaporation; Watermark defect

1. Introduction

For higher performance, higher functionality, and lower power consumption of the next generation semiconductor devices, pattern size is scaled down, while the chip area and the wafer size as well as the number of processes for the fabrication are increased. Wafer cleaning processes occupy more than 30% of the total manufacturing processes, and the number of the cleaning processes is likely to increase with the increased number of total processes.

The conventional wafer cleaning processes, which use the multi-wafer-immersion cleaning tanks with megasonic physical force, become hard to meet the reinforced specifications. Megasonic physical force is not applicable to fine patterns, since it may cause pattern collapse. Small particles, which were not classified as sources of defects in the conventional large pattern fabrication processes, may work as defect sources in the recent fine pattern fabrication processes. To maintain the yield of the chips of increased area, the allowable number density of defects decreases in inversely proportional to the increased area ratio [1].

Recently, single wafer cleaning processes are introduced in the microelectronics fabrication to tackle the particle contamination challenge due to higher particle removal efficiency and lower particle reattachment possibility. In single wafer cleaning processes, wafers are spinning at high speed, and water is supplied on the wafers to rinse the wafer and remove the etched-out particles. Water in the liquid film is replaced with *iso*-propyl alcohol (IPA) to stop oxygen attack on silicon, while the eluted particles are removed away by the radial liquid film convection which is caused by the centrifugal force. However, some trials to adopt the single wafer cleaning process end up with failures, and the reasons are not explained clearly yet.

Olim [2] classified the silicon wafer processing into four distinct stages as feature wetting, chemical transport into

* Corresponding author. Present address: Department of Mechanical Engineering, College of Advanced Technology, Kyunghee University 1, Seocheon-dong, Giheung-ku, Yongin-si, Gyunggi-do 446-701, South Korea. Tel.: +82 31 201 3834; fax: +82 31 202 8106.
E-mail address: jmkoo@khu.ac.kr (J. Koo).

0017-9310/$ - see front matter © 2007 Elsevier Ltd. All rights reserved.
doi:10.1016/j.ijheatmasstransfer.2007.02.043

Nomenclature

c	volume fraction (–)	t	time (s)
d	diameter (m)	u, v, w	velocity (component) (m/s)
D	diffusivity (m^2/s)	z	coordinate (m)
f	function (–)		
g	gravity acceleration (m^2/s)	*Greek symbols*	
h	film thickness (m)	μ	dynamic viscosity (Pa s)
k	mass transfer coefficient (m/s)	ν	kinematic viscosity (m^2/s)
m	mass (kg)	ρ	density (kg/m^3)
M	molar mass (kg/kmol)	τ	stress (Pa), time scale (s)
N	number of solvent species (–)		
p	pressure (Pa)	*Superscripts/subscripts*	
r	radial coordinate (m)	0	initial value
Re	Reynolds number (–)	A	species
RH	relative humidity (%)	eq	equilibrium
Sc	Schmidt number (–)	i, j	index
Sh	Sherwood number (–)	sat	saturation

and out of the feature, and drying stages. He calculated the time scales of the dominating mechanisms of these stages and reported that they are significantly shorter than the process time scale for hydrophilic surfaces. The importance of drying phase on the watermark defects has been reported by Leenaars et al. [3], Mertens et al. [4], and Lauerhaas et al. [5], where they proposed to use the "Marangoni" and "Rotagoni" dry which use rotational and Marangoni forces to reduce the defects. Lin et al. [6,7] investigated the cleaning of surfaces and submicron deep trenches using physical numerical modeling. They reported that the pulsating (megasonic) flow rinse shows a significant advantage over steady flow rinse. Qin and Li [8] proposed a quantitative mechanism of particle removal from silicon wafer surface by a wet chemical cleaning process considering the combined effects of chemical etching and a net repulsive interaction between the particle and surface. Hirota et al. [9] and Hirano et al. [10] introduced a wafer cleaning system adopting water and gas mixture jet to avoid the pattern collapse problem.

In this study, the origins of watermark defects in single wafer cleaning system were identified, and the ways to avoid the problems were suggested through a model based numerical simulation. The new findings provide important guidelines to improve existing single wafer cleaning systems.

2. Theory

Fig. 1 compares from rinsing to drying phases between the real single wafer cleaning system and the simulation model currently used. After the chemical treatment on the wafer surfaces, wafers are rinsed by water. The water film on the wafer is then replaced with IPA to suppress oxygen attack on silicon, and the residual film drying phase follows.

2.1. Governing equations

The generalized governing equations for incompressible fluid flows over a disk can be written as [11]:

Continuity equation:

$$\nabla \cdot \vec{v} = 0 \tag{1a}$$

Momentum equation:

$$\rho \frac{\partial \vec{v}}{\partial t} + (\vec{v} \cdot \nabla)\vec{v} = -\nabla p + \rho \vec{g} - \nabla \cdot \vec{\vec{\tau}} \tag{1b}$$

Concentration transport equation:

$$\frac{\partial c_i}{\partial t} + (\vec{v} \cdot \nabla)c_i = \nabla \cdot (D \nabla c_i) \tag{1c}$$

where $\vec{v}$ is the velocity vector, ρ is the fluid density, p is the pressure, $\vec{\vec{\tau}}$ is the stress tensor, $\vec{g}$ is the gravity acceleration vector, c_i is the (volume) fraction of species i, and D is the diffusivity of species i.

Flack et al. [12], Bornside et al. [13], Lawrence [11], Ohara et al. [14], Bornside et al. [15], Yonkoski and Soane [16], Tortai [17] derived the simplified form of Eq. (1) to investigate spin coating processes, where a drop of solution is dispensed and coated on a rotating wafer to form an uniform photoresist film for the lithography stages of microelectronic manufacturing processes. They considered the force balance between the centrifugal and viscous forces acting on the film, and the mass balance between convection, diffusion and evaporation of solvents in the film. In this study, the same set of equations is used. While the concentration dependence of the diffusivity $D(c_A)$ in Eq. (1c) makes the equation highly non-linear and hard to integrate, it could be assumed to be constant for single wafer cleaning processes where the solute contents are extremely low. Furthermore, the species, e.g., water and IPA, in the liquid film were assumed to be well-mixed, and the validity

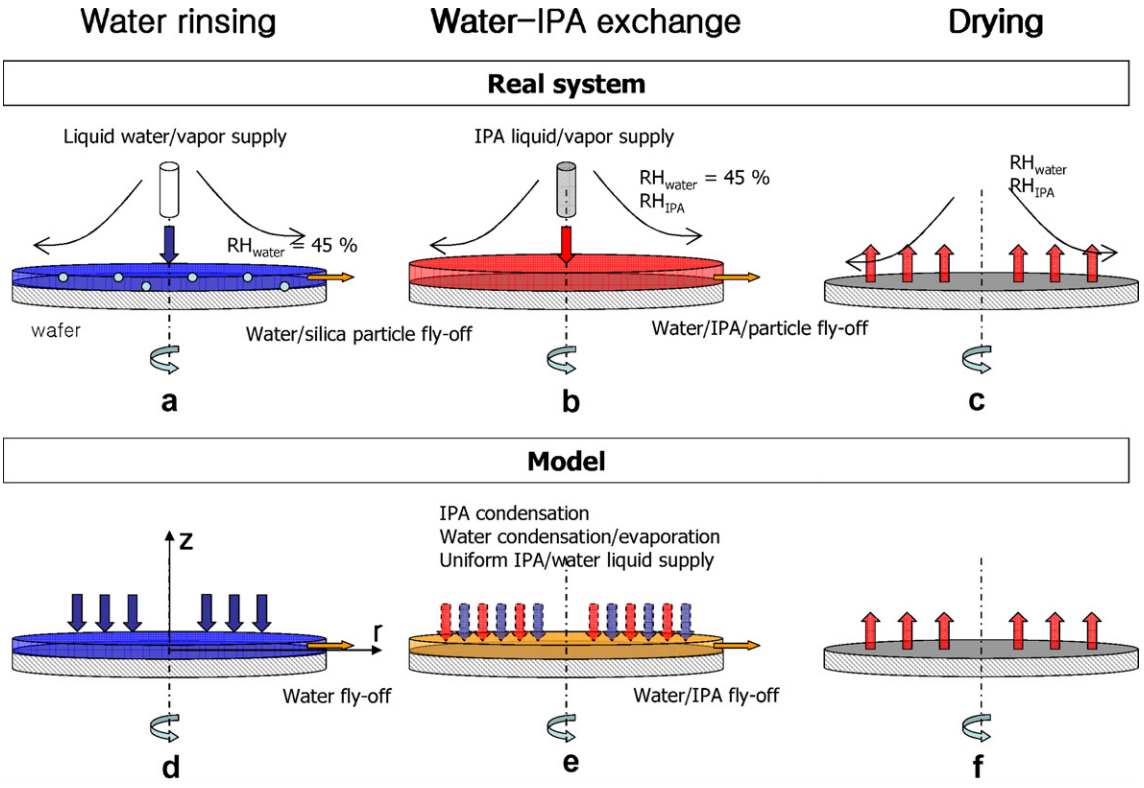

Fig. 1. Comparison of real process and simulation model: (a) and (d) water rinsing phase, (b) and (e) water–IPA substitution phase, and (c) and (f) drying phase.

is discussed in Section 3.2.3. The film thickness was assumed to be uniform neglecting the variation in the radial direction. Comparing the time scales for evolutions of the velocity and concentration fields, Lawrence [11] reported that the velocity field develops much faster than the concentration field does, so that the velocity field could be assumed to be always in steady state and neglect the time dependent term in Eq. (1b). The one-dimensional form of Eq. (1) reads

$$u = rf_z(z,t), \quad w = -2f(z,t) \tag{2a}$$

$$(vf_{zz})_z = -1 \tag{2b}$$

$$\frac{\mathrm{d}h}{\mathrm{d}t} - w|_{z=h(t)} + k\sum_j^N \frac{\rho_{\mathrm{air}}}{\rho_{j,\mathrm{liquid}}}\frac{M_j}{M_{\mathrm{air}}}(c_j|_{z=h} - c_{j,\infty}) = 0 \tag{2c}$$

$$c_i = \frac{m_i/\rho_i}{\sum_j^N m_j/\rho_j} \tag{2d}$$

$$\dot{m}_i''/\rho_{\mathrm{air}} = k(c_i|_{z=h(t)} - c_{i\cdot\infty}) \tag{2e}$$

where u and w are the velocity components in r- and z-directions, and f, v, h, k, N, M, $c_i|_{z=h(t)}$ and $c_{i\cdot\infty}$ are a function, the kinematic viscosity, film thickness, mass transfer coefficient, number of species in the film, molecular weight, vapor (volume) concentration at the interface and in the surrounding gas. The subscript z in Eqs. (2a) and (2b) represents the differentiation of the function f in the z-direction. Although the effective kinetic viscosity of water and IPA mixture varies depending on its composition, it was assumed to be constant, and equals to the value of water.

The number of space intervals between wafer surface ($z = 0$) and the film-gas interface ($z = h(t)$) was kept constant, and uniform spacing was used ($\Delta z = h(t)$/number of meshes). The uniform meshes were updated every time step to consider the change of the interface location due to the fly-off and evaporation of liquids [18].

2.2. Boundary conditions

The boundary and initial conditions are listed below.

$$u = w = 0 \quad \text{at } z = 0 \tag{3a}$$

$$\frac{\partial c_A}{\partial z} = 0 \quad \text{at } z = 0 \tag{3b}$$

$$\frac{\partial u}{\partial z} = 0 \quad \text{at } z = h(t) \tag{3c}$$

$$h(t=0) = h_0 \tag{3d}$$

$$c_A(t=0) = c_0 \tag{3e}$$

where $\frac{\dot{m}''}{\rho}$ represents the evaporative-volume flux, which could be calculated as

$$\frac{\dot{m}_i''}{\rho_{\mathrm{air}}} = k\frac{M_i}{M_{\mathrm{air}}}(c_A|_{z=h(t)} - c_{A,\infty}) \tag{3f}$$

Here, the mass transfer coefficient k and the volume fraction at the interface c_A are needed to be determined to close the problem.

The mass transfer coefficient k for steady laminar flow on the spinning disk can be obtained from the relation below [19]:

$$Sh = \frac{kd_{\text{disk}}}{2D} = 0.879Re^{1/2}Sc^{1/3} \tag{4}$$

where Sh, Re, and Sc are Sherwood number, Reynolds number $\left(\equiv \frac{\omega d_{\text{disk}}^2}{2\nu_{\text{air}}}\right)$, and Schmidt number $\left(\equiv \frac{\nu_{\text{air}}}{D}\right)$. The mass transfer coefficient is independent of the radial position for laminar flow [16], while it is radial position dependent for turbulent flow [20]. Therefore, the one-dimensional model, which cannot capture the effect of non-uniform evaporation on film profile, is only applicable to laminar flow cases. For a 12 in. spinning wafer, the gas flow over it is laminar up to 1700 rpm [21]. In this study, the flow was assumed to be laminar in any case.

The volume fraction at the interface $c_A|_{z=h(t)}$ could be evaluated by applying Raoult's law, which estimates the mole, or volume, fraction of a species on the liquid and gas sides of the interface under thermodynamic equilibrium [19]. The vapor and the liquid-phase water–IPA mixture are assumed to be an ideal gas and ideal solution. Then, the vapor volume fraction of a species i at the interface could be expressed as:

$$c_i|_{z=h(t)} = x_i \frac{p_i^{\text{sat}}}{p} \tag{5}$$

where x_i is the mole fraction of species i in the liquid film, p_i^{sat} is the saturation pressure of the species i at the interface temperature, and p is the total pressure on the gas-phase side. Thus, water and IPA can either evaporate from the liquid film or condense into it depending on the sign of the difference between concentrations at the interface and in the surrounding gas. During the cleaning process, pure water could be replaced with *iso*-propyl alcohol by raising the relative humidity of IPA such that IPA condenses into the liquid film, while water evaporates out of it. In a clean room for the semiconductor fabrication, downflow is adopted to prevent particle contamination. The downflow usually holds water vapor, and its relative humidity is about 45%, which sets the boundary conditions for the concentration of water vapor in the surrounding gas.

3. Results and discussion

3.1. Analysis of basic mechanism

Yonkoski and Soane [16] compared the effects of convective and evaporative mass flowrates on film thinning in the spin coating process. It is easy to compare the impacts of convection and evaporation on the average liquid film thickness by comparing the convective and evaporative mass flowrates ($\dot{m}_{\text{c}}$ and $\dot{m}_{\text{e}}$) of liquids leaving the film on a wafer (see Fig. 2). The convective mass flowrate $\dot{m}_{\text{c}}$ indicates the rate of mass ejection at the edge of wafer by means of liquid convection. The evaporative mass flowrate $\dot{m}_{\text{e}}$ is the rate of mass leaving the liquid film on wafer by means of evaporation. They reported that film thins out at a very high rate due to the force of the centrifugal acceleration in the initial phase, and at a lower rate by solvent evaporation in the later phase. Fig. 3, which reproduced the observations of Yonkoski and Soane [16], shows the effects of the relative humidity on water film thickness evolution. It took longer for a film to dry out under higher relative humidity conditions. Initially, the effects of relative humidity were hardly noticed, where the evaporative flux was negligible compared to the convective flux. The IPA films dried up faster than water films due to higher evaporation flux of IPA. The convective- and evaporative-volume flowrates are compared in Fig. 4 for a water film on a spinning disk. Initially, the convective-volume flowrate was greater than the evaporative-volume flowrate, and the impact of the evaporative part on total thinning rate was negligible until around 2 s. The convective flowrate decreased as film thickness decreased because the ratio of the centrifugal to viscous force is inversely proportional to h^2. For a given vapor relative humidity condition, the evaporative flux remained constant, and became main mechanism of film thinning in a later phase ($t > 7$ s). The evaporative flux decreased with the relative humidity, since the concentration difference driving evaporation decreases in Eq. (3f). The data for relative humidity of 100% case are not shown in Fig. 4, because the convective flowrate was very close to that for $\text{RH}_{\text{water}} = 80\%$ case, and the evaporative flowrate was zero.

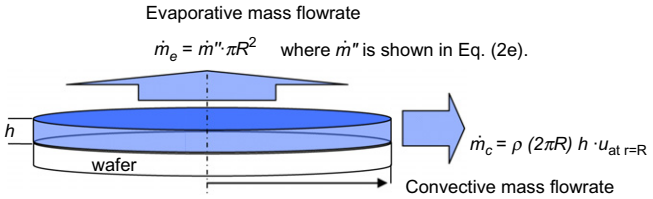

Fig. 2. Description of convective- and evaporative flowrates.

3.2. Water–IPA exchange phase

The water–IPA exchange can be done by supplying IPA either in gas- or in liquid-phase. For the cases of gas-phase supply, the gas-phase exchange is performed by letting the gas-phase *iso*-propyl alcohol diffuse into the water film from the film-gas interface ($z = h(t)$). There is a trade-off between the diffusion for the exchange and the convection for the particle removal – thin film thickness facilitates the diffusion, while it hinders the convection. The film thickness should be thick enough to remove the particles efficiently, while it should be thin enough to replace water with IPA in short time.

When IPA is supplied in liquid-phase, water is directly replaced with incoming IPA, and the eluted silica particles are removed by the radial liquid convection. The liquid-phase IPA supply may be a better choice, since the exchange can be done in shorter time while keeping the liquid film thick. To investigate the liquid injection effect, it was

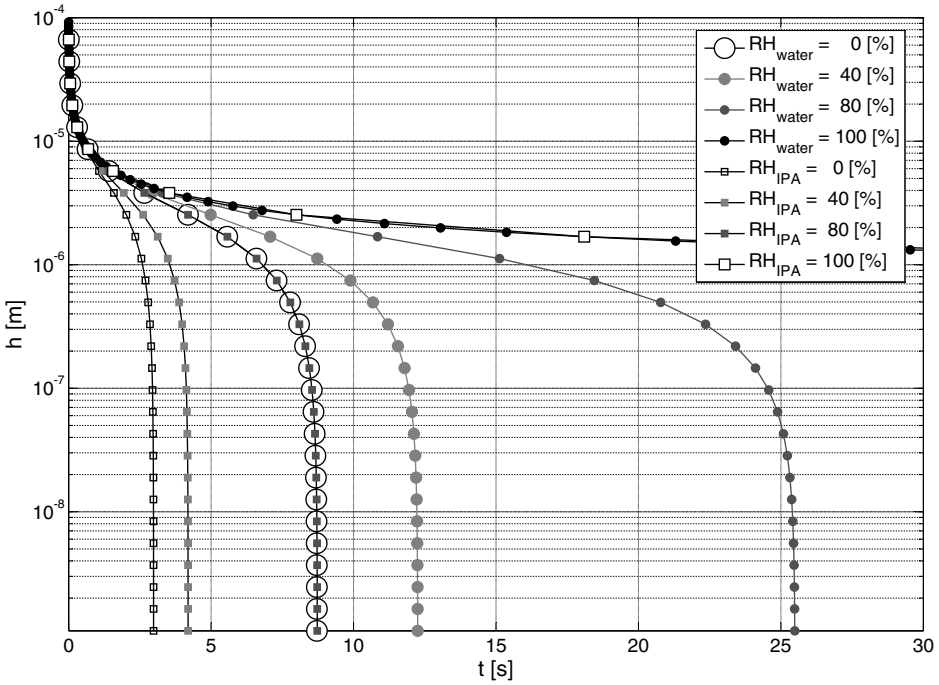

Fig. 3. Effects of relative humidities on pure water ($c_{IPA} = 0$) and IPA ($c_{IPA} = 1$) film thickness evolutions: $h_0 = 100$ μm and $\omega = 1000$ rpm.

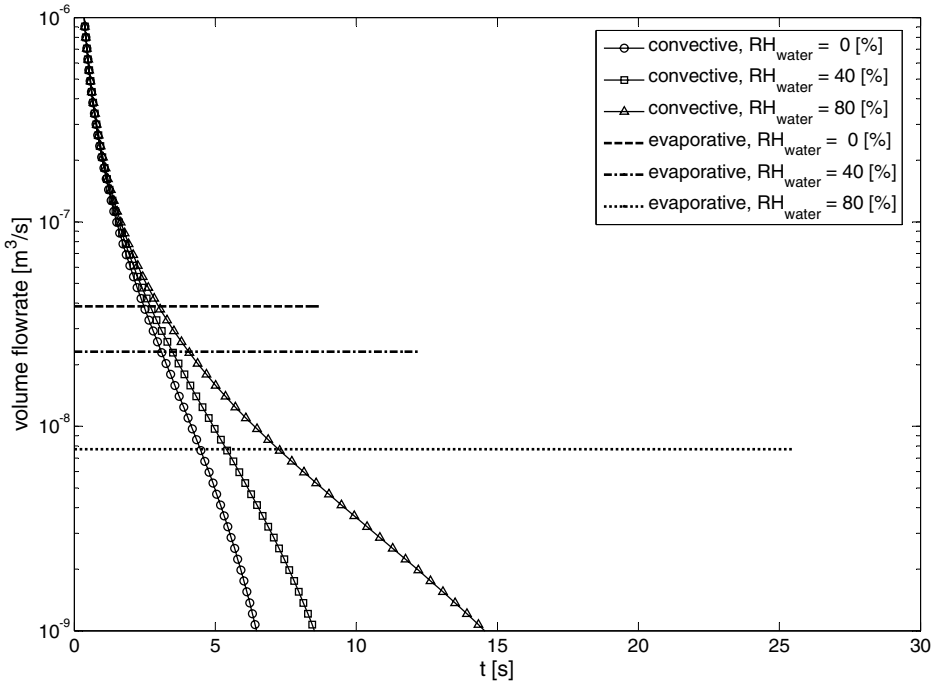

Fig. 4. Comparison of convective- and evaporative-volume flowrates of a water film: $h_0 = 100$ μm and $\omega = 1000$ rpm.

assumed that the injected IPA liquid is uniformly distributed to the liquid film on a whole wafer. Thus, the volume flux can be estimated as $\dot{V}''_{IPA,injected} = \dot{V}_{IPA,injected}/(\pi R^2)$.

3.2.1. Effects of relative humidities on equilibrium film thickness

In Section 3.1, the films dried up in the end for the case of single component liquid film. The liquid film should remain covered on the wafer during the exchange phase to remove the eluted silica particles. To stop the particle elution and sustain the liquid film thickness, it is necessary to maintain high relative humidity of IPA, when IPA is supplied in gas-phase. The condensing rates of IPA and water across the liquid–gas interface during the exchange phase match the flowrates of them leaving the film through convection in the equilibrium state (see Fig. 5). Initially, the

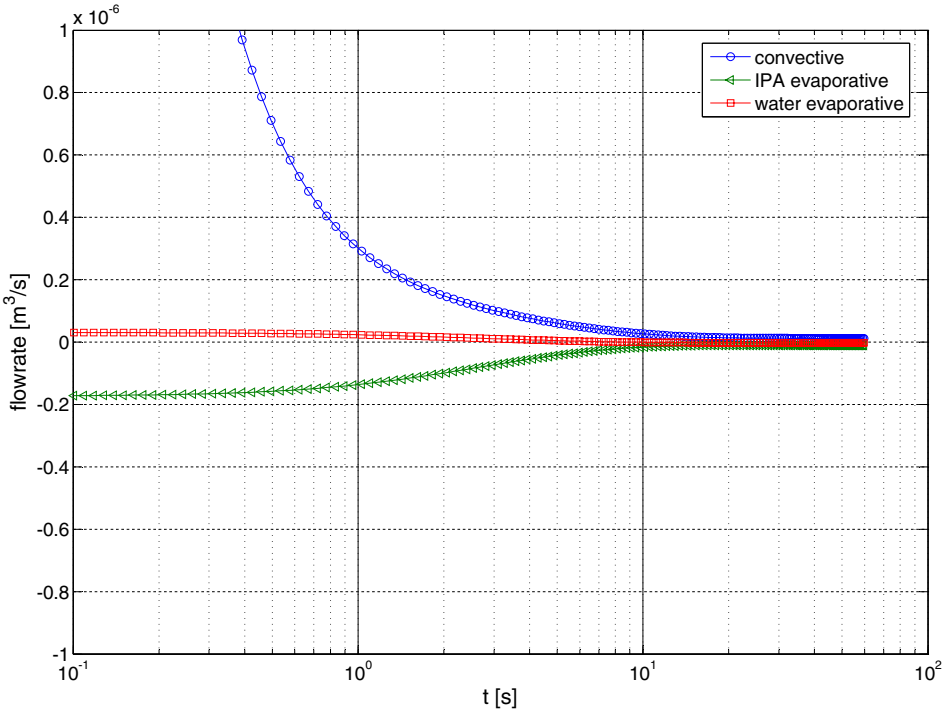

Fig. 5. Comparison of convective, condensation flowrates during water–IPA exchange phase: $\omega = 1000$ rpm, $RH_{IPA} = 90\%$, $RH_{water} = 20\%$, $h_0 = 100$ μm, and $h_{eq} = 2.7$ μm.

total convective flowrate decreased rapidly. Water slowly evaporated out, and IPA condensed into the liquid film increasing its content in the film. Shortly, water started to condense, and the total condensation flowrate balanced with the convective flowrate. When the surrounding gas is IPA saturated, or when relative humidity is 100%, the volume fraction of the IPA vapor in surrounding gas is $c_{IPA} = p^{sat.}_{IPA}/P$, where $p^{sat.}_{IPA}$ is the saturated vapor pressure of IPA for the given temperature, and P is the total pressure. For single component systems, the vapor pressure at the interface between IPA liquid film and surrounding gas could be calculated from Eq. (5) where x_{IPA} is unity. This means no evaporation or condensation could happen under 100% relative humidity condition. For two component systems, the IPA mole fraction in liquid film x_{IPA} is lower than unity due to the existence of water, so that the IPA vapor pressure at the interface is less than the saturated vapor pressure. Then, the IPA vapor volume fraction at the interface is lower than that in the saturated surrounding gas, and IPA vapor condenses into the IPA–water mixture liquid film. The condensing IPA supplies additional liquid to compensate the drainage of liquid film by centrifugal force. This indicates that the water- and IPA vapors could condense into liquid film when the relative humidities of them are high enough as shown in Figs. 6 and 7.

Fig. 6 shows the effects of relative humidities of water and IPA, and disk spin speed on the equilibrium film thickness, $h_{equilibrium}$. The equilibrium film thickness increased with the relative humidities, and decreased with the disk spin speed. The evaporative flux decreased and the condensation flux increased with the relative humidities resulting in thicker films. Although the thinning effect of centrifugal force also increased with film thickness, the impact of the condensation outweighed it. Note that the real equilibrium film thickness should be thicker than shown in Fig. 6, because the viscosity of IPA was assumed to be the same with that of water for simplification, while it is about twice larger. The c_{IPA} in Fig. 6 represents the volume fraction of IPA in the film in equilibrium. It depended strongly on the relative humidities of water and IPA. The IPA concentration in the film increased with the relative humidity of IPA, since the concentration difference in Eq. (3f) increased to result in high condensation flux.

When IPA is delivered in liquid-phase, the effect of IPA liquid injection on film thickness, interfacial velocity, and IPA volume fraction in the film at equilibrium are shown in Table 1. With a small amount of liquid IPA supply, e.g., 1 cc/s, the equilibrium film thickness could be increased to 11 μm. When the amount of the injection was doubled, the film thickness was increased by 30% to 14.5 μm, because the increased impact of centrifugal force mitigated the film thickness increase.

3.2.2. Effects of relative humidities on particle removal

The eluted silica particles diffuse out of features such as trenches, vias, and topology, and are conveyed away by the radial convection. Since the particle size is very small ($\mathcal{O}$ (1–10 nm)), the velocity response time $\left(\tau_v = \frac{\rho d_p^2}{18\mu}\right)$ is so small that the particles can be assumed to travel at the speed of

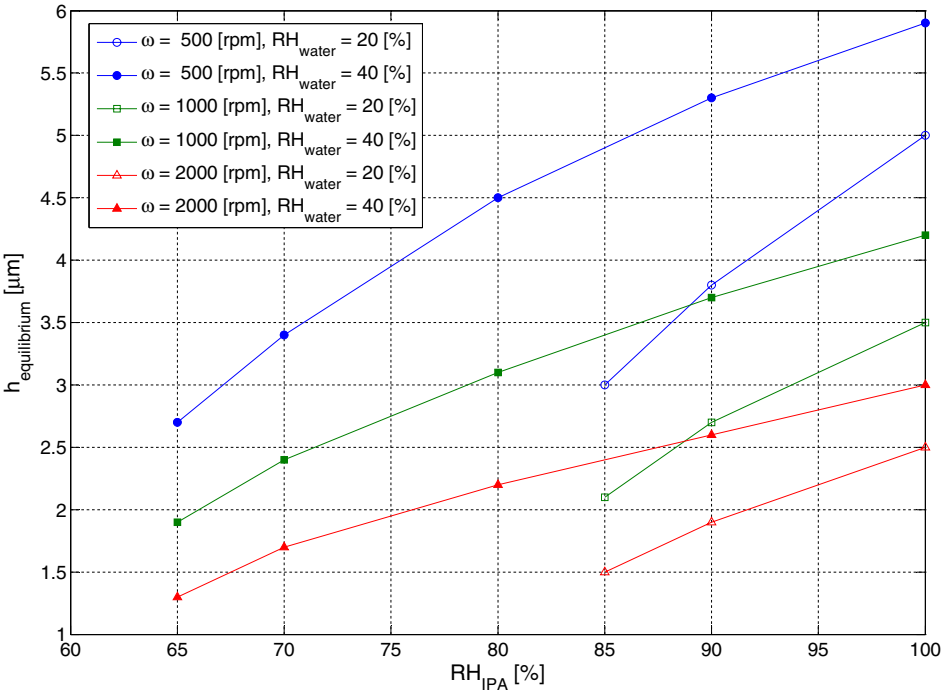

Fig. 6. Effects of relative humidities on equilibrium film thickness.

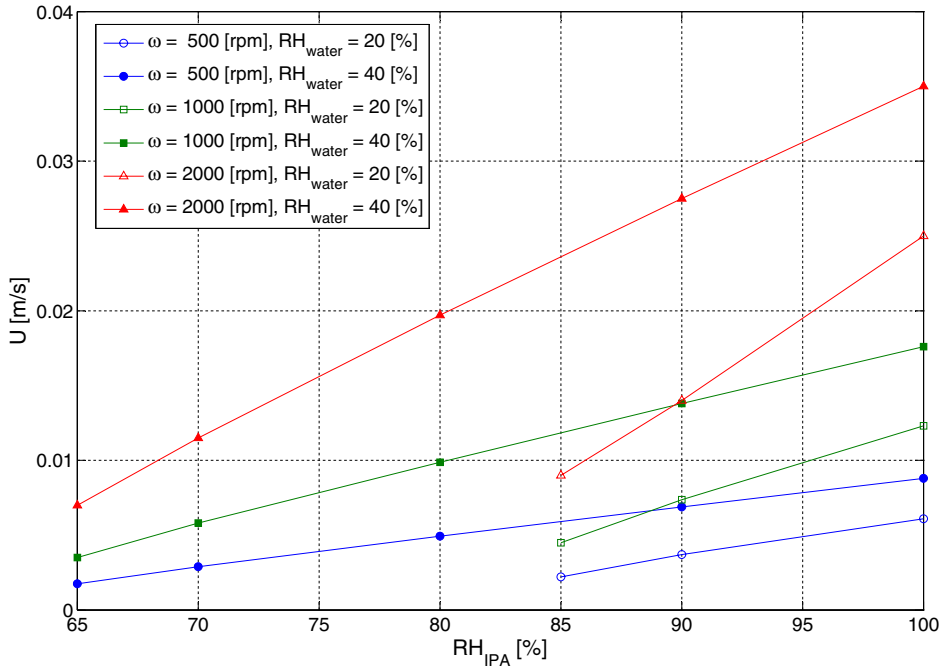

Fig. 7. Effects of relative humidities on the interfacial radial velocity of liquid film.

liquid flow. For the efficient particle removal, the convection speed in the film should be high enough.

The effects of relative humidities and disk spinning speed on the film radial flow velocity at the interface, $U = u|_{z=h(t)}$, are shown in Fig. 7. The film flow velocity increased with the relative humidities and disk spinning speed. Higher relative humidities yielded thicker liquid film. The interfacial radial velocity U can be expressed as

$$U \sim \frac{\rho r \omega^2 h_{eq}^2}{\mu} \tag{6}$$

For a given disk spinning speed, the interfacial radial velocity increases in proportion to h^2. It was observed that the interfacial velocity was greater for the spinning speed of 1000 rpm cases than 500 rpm cases, although the film was thicker for 500 rpm cases, which could be attributed to

Table 1
Effects of IPA liquid injection rate on equilibrium film thickness, $h_{equilibrium}$, interfacial flow speed, U, and the IPA volume fraction in the film, c_{IPA}; $\omega = 1000$ rpm, $RH_{water} = 40\%$, $RH_{IPA} = 0\%$, $R = 0.15$ m

Injection rate (cc/s)	$h_{equilibrium}$ (μm)	U (cm/s)	c_{IPA} (–)
1	11	12	0.98
2	14	21	0.99

the stronger interfacial velocity dependence on the disk spinning speed compared to that on the film thickness which is determined by the balance between the condensation and the radial convection flowrates.

According to Table 1, the liquid injection enhances the radial convection. The interfacial velocity increased to 11 cm/s with the IPA injection of 1 cc/s, which resulted in efficient particle removal.

3.2.3. Effects of relative humidities on the water–IPA exchange

While the silica particles are removed off the wafer, water in the cleaning film should be replaced with *iso*-propyl alcohol to stop the elution of silica particles from the wafer. The water–IPA exchange process is assumed as pure diffusion process, when IPA is supplied in gas-phase. The time scale for the diffusion process can be estimated as

$$\tau_{exchange} = \frac{h_{eq}^2}{D} \tag{7}$$

For liquids, typical binary diffusivity is in the order between $\mathcal{O}(10^{-8})$ and $\mathcal{O}(10^{-10})$ (m^2/s) [19]. Table 2 compares the time scales for the diffusion process to exchange water and *iso*-propyl alcohol. The diffusivity is assumed to be 10^{-9} m^2/s. Note that the exchange can be done within reasonable time, e.g., 1 s, when the film is thinner than 10 μm. However, it takes too long for thick film ($h_{eq} = 100$ μm) considering that the whole cleaning process should be done within 30–60 s. This confirms the validity of the well-mixing assumption applied in Eq. (2d); the operation duration is at least an order longer than the time required for mixing.

Referring to Table 1, the IPA liquid injection promotes water–IPA exchange, since liquid IPA is directly supplied to the film.

As discussed both in Sections 3.2.2 and 3.2.3, it is found that higher liquid film convection speed and thinner film are desirable for the water–IPA exchange process. It is recommended to spin at a high speed to meet the two requirements in the water–IPA exchange phase for gas IPA supply cases. The relative humidity of *iso*-propyl alcohol should be set so high that its concentration in the film should be kept high enough to stop the silica elution, while water relative humidity should be kept as low as possible to increase IPA contents in the film. The liquid-phase IPA injection is found to be beneficial in terms of both particle removal and water–IPA exchange efficiencies.

Table 2
Comparison of time scales for the water–IPA exchange processes for different equilibrium film thickness; $D = 10^{-9}$ m^2/s

h_{eq} (μm)	$\tau_{exchange}$ (s)
1	10^{-3}
10	10^{-1}
100	10

3.3. Drying phase

3.3.1. Effects of initial iso-propyl alcohol concentration in the liquid film

Fig. 8 shows the effects of initial concentration on the evolution of IPA concentration in the liquid film under the condition that the relative humidity of IPA is zero. Here, the terms, "initial concentration" and "initial film thickness", mean the equilibrium concentration and the equilibrium film thickness h_{eq} of the water–IPA exchange phase. The *iso*-propyl alcohol concentration decreased as the film thins out, so that only water remained in the final phase of the drying process. Even pure IPA films changed into pure water films. Two initial film thickness conditions, 100 and 1000 μm, were tested, and they gave the same results. In the absence of IPA in the liquid film, the elution of silica particle cannot be stopped, which may result in watermark defects. Fig. 9 shows the comparison of evaporative flowrates of water and IPA. Initially, water condensed into the liquid film, while IPA evaporated out. As film thinned about to 1 μm, IPA completely escaped from the film, and only water remained. Then, the water film dried out completely.

It was found that increasing initial IPA concentration alone could not prevent the watermark defects. This explains the reason why the single wafer cleaning systems which were not equipped with the relative humidity control systems failed to avoid watermark defects.

3.3.2. Effects of iso-propyl alcohol relative humidity

The final IPA concentration, $c_{IPA,final}$ of the liquid film at the end of the drying phase could be increased by increasing the relative humidity of IPA in the surrounding gas as shown in Fig. 10. The concentration increased almost linearly with the relative humidity of *iso*-propyl alcohol. When the relative humidities were high enough, the films did not dry up; such conditions are marked with the letter 'F' in Fig. 10. The film forming relative humidity values of IPA decreased, as the relative humidity of water increased. The effects of the water relative humidity was relatively weak compared to the effects of the IPA relative humidity. The final concentration was found to be independent of the wafer spinning speed. The relative humidity conditions for the defect-free wafer cleaning should be set depending on the required level of IPA concentration in

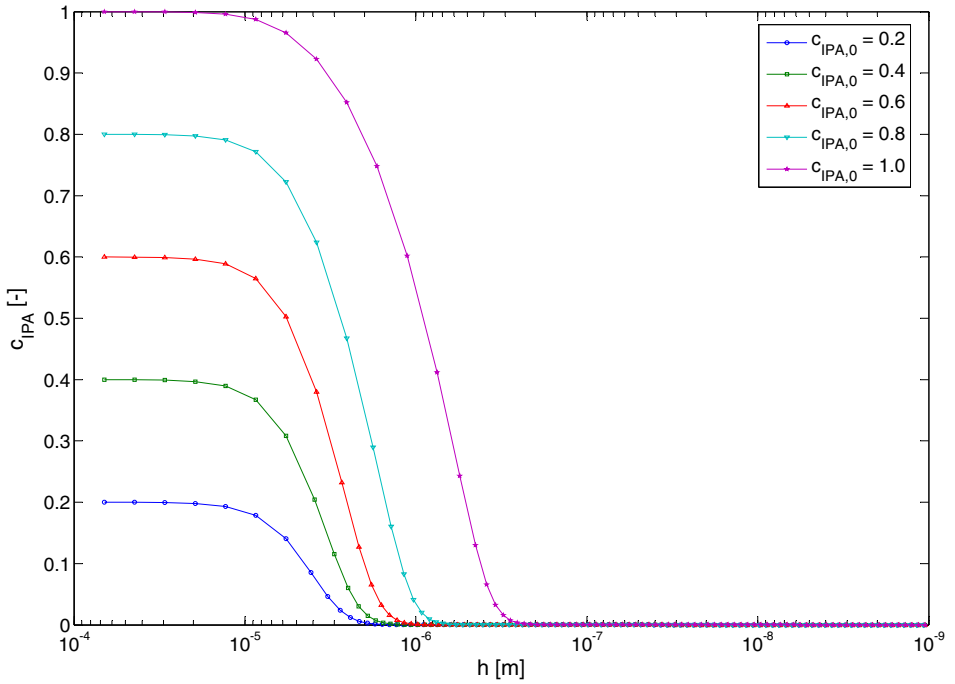

Fig. 8. *iso*-Propyl alcohol concentration evolution in liquid film: $\omega = 1000$ rpm, $RH_{water} = 45\%$, $RH_{IPA} = 0\%$.

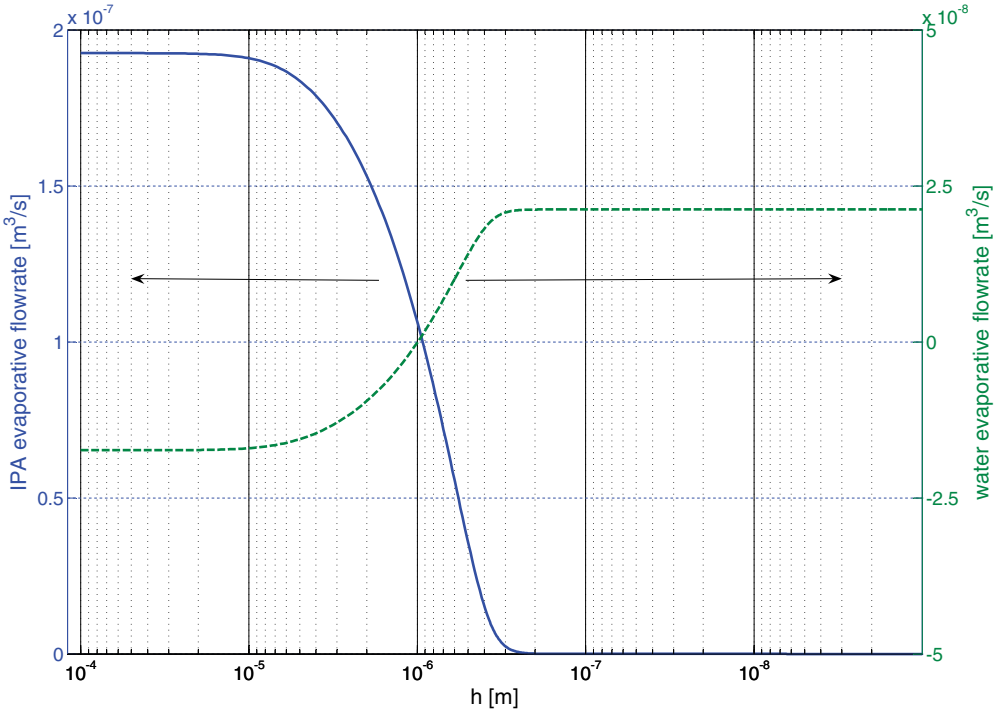

Fig. 9. Comparison of evaporative flowrates of water and *iso*-propyl alcohol in the drying phase: $\omega = 1000$ rpm, $RH_{water} = 45\%$, $RH_{IPA} = 0\%$.

the film, e.g., $c_{IPA} = 0.6$, where the silica particle elution stops.

The effects of initial IPA concentration in the film and the relative humidity of IPA on the film drying time are shown in Fig. 11. The drying time increased with initial water concentration and IPA relative humidities. The film thicknesses decreased very fast initially, the thinning rates decreased drastically. The thinning rate depended on the composition of the film. Films of higher IPA concentration evaporate faster. In Fig. 11, the thinning rates for

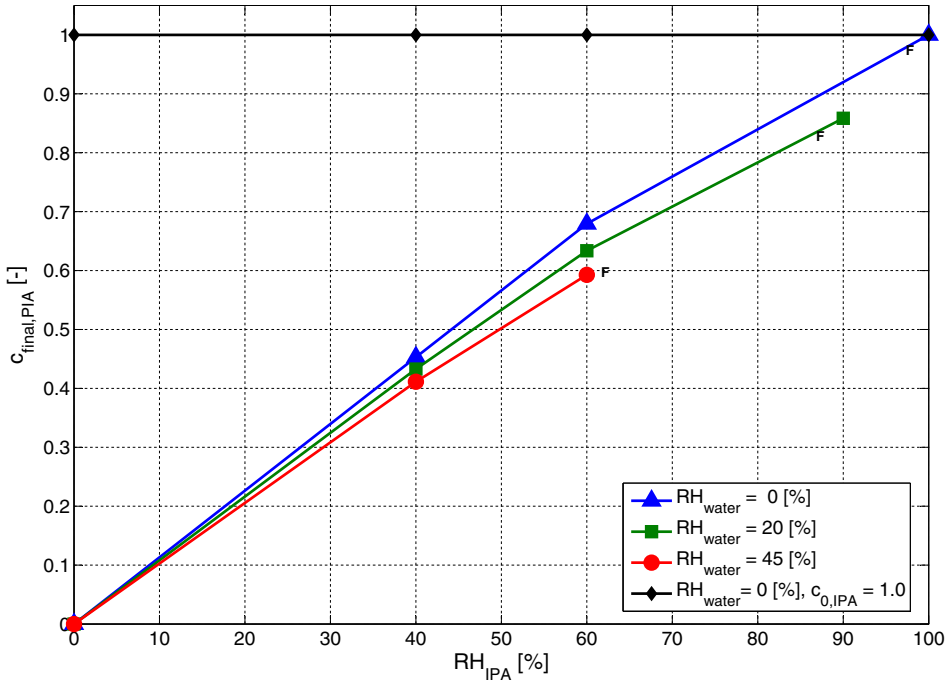

Fig. 10. Effects of water and *iso*-propyl alcohol relative humidities on the *iso*-propyl alcohol concentration in the film at the end of the drying phase. The letters 'F' in the graph represents film forming conditions: $h_0 = 100$ μm.

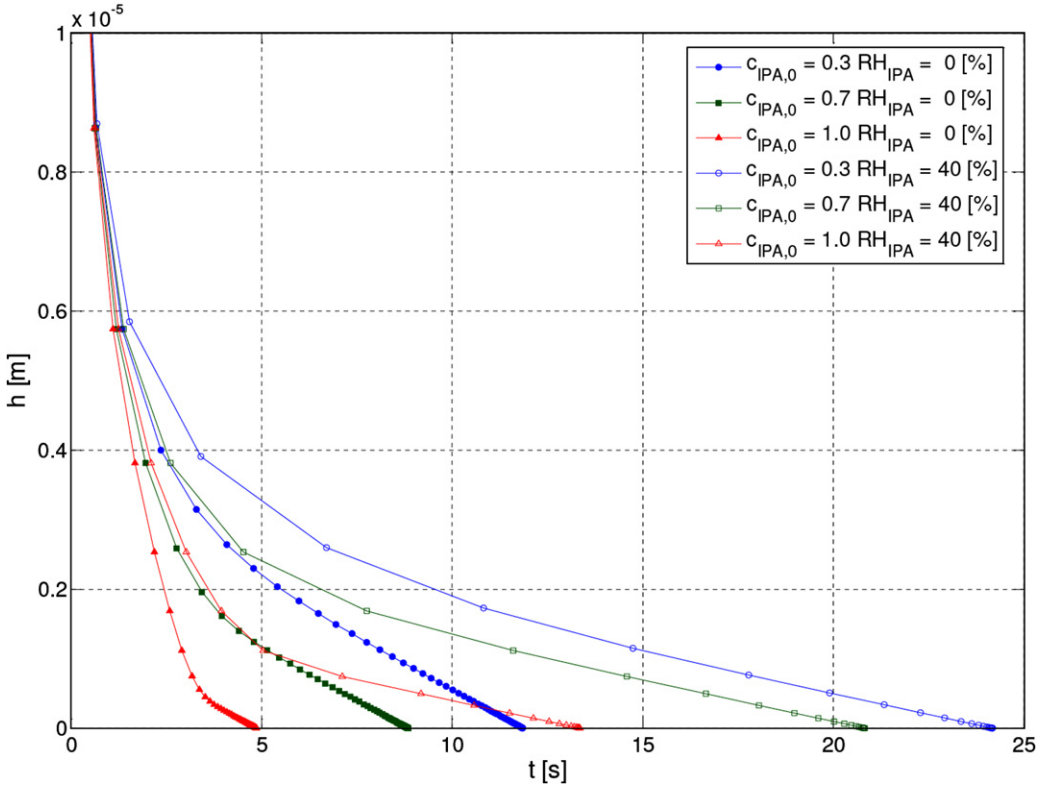

Fig. 11. Effects of water and *iso*-propyl alcohol relative humidities on the film drying time: $\omega = 1000$ rpm, $h_0 = 100$ μm, $RH_{water} = 45\%$.

given relative humidities conditions became the same at the final stage of the drying process. At the final stage, the film composition is determined by the relative humidities of water and IPA, and the evaporation or thinning rates should be equal for given water and IPA relative humidities.

4. Conclusions

The following conclusions can be drawn from this model based numerical study. The watermark defects observed in the single wafer cleaning systems were found to originate from the failure of controlling water and *iso*-propyl alcohol relative humidities in the surrounding gas. During the water–IPA exchange phase, the relative humidities of water and *iso*-propyl alcohol, and wafer spinning speed needed to be kept high enough for efficient particle removal and fast water–IPA exchange, when IPA was supplied in gas-phase. The liquid-phase IPA injection was found to be beneficial in terms of both particle removal and water–IPA exchange efficiencies. Increasing the *iso*-propyl alcohol relative humidity in the surrounding gas during the water–IPA exchange and drying phases can improve the watermark defects and increase product yields.

References

[1] R.C. Jaeger, Introduction to Microelectronic Fabrication, second ed., Prentice Hall, 2002.
[2] M. Olim, Liquid-phase processing of hydrophilic features on a silicon wafer, J. Electrochem. Soc. 144 (1997) 4331–4335.
[3] A.F.M. Leenaars, J.A.M. Huethorst, J.J. van Oekel, Marangoni drying: a new extremely clean drying process, Langmuir 6 (1990) 1701–1703.
[4] P.W. Mertens, G. Doumen, J. Lauerhass, K. Kenis, W. Fyen, M. Meuris, S. Arnauts, K. Devriendt, R. Vos, M. Heyns, A high performance drying method enabling clustered single wafer wet cleaning, in: Symposium on VLSI Technology Digest of Technical Papers, Honolulu, HI, June, 2000, IEEE, 2000, pp. 56–57.
[5] J. Lauerhaas, P.W. Mertens, W. Fyen, K. Kenis, M. Meuris, T. Nicolosi, M. Bran, B. Fraser, C. Franklin, Y. Wu, M. Heyns, Single wafer cleaning and drying: particle removal via a non-contact, non-damaging megasonic clean followed by a high performance "rotagoni" dry, in: The Ninth International Symposium on Semiconductor Manufacturing, September, 2000, IEEE, 2000.
[6] H. Lin, A.A. Busnaina, I.I. Suni, Physical modeling of rinsing and cleaning of submicron trenches, in: IEEE 2000 International Interconnect Technology Conference, Burlingame, CA, June, 2000.
[7] H. Lin, A.A. Busnaina, I.I. Suni, Cleaning of high aspect ratio submicron trenches, in: IEEE/SEMI Advanced Semiconductor Manufacturing Conference, 2002.
[8] K. Qin, Y. Li, Mechanisms of particle removal from silicon wafer surface in wet chemical cleaning process, J. Colloid Interf. Sci. 261 (2003) 569–574.
[9] Y. Hirota, I. Kanno, K. Fujiwara, H. Nagayasu, S. Shimose, Damage-free wafer cleaning by water and gas mixture jet, in: IEEE International Symposium on Semiconductor Manufacturing, September, 2005, pp. 219–222.
[10] H. Hirano, K. Sato, T. Osaka, H. Kuniyasu, T. Hattori, Damage-free ultradiluted hf/nitrogen jet spray cleaning for particle removal with minimal silicon and oxide loss, Electrochem. Solid-State Lett. 9 (2006) G62–G65.
[11] C.J. Lawrence, The mechanics of spin coating of polymer films, Phys. Fluids 31 (1988) 2786–2795.
[12] W.W. Flack, D.S. Soong, A.T. Bell, D.W. Hes, A mathematical model for spin coating of polymer resists, J. Appl. Phys. 56 (1984) 1199–1206.
[13] D.E. Bornside, C.W. Macosko, L.E. Scriven, On the modeling of spin coating, J. Imaging Technol. 13 (1987) 122–130.
[14] T. Ohara, Y. Matsumoto, H. Ohashi, The film formation dynamics in spin coating, Phys. Fluids A 1 (1989) 1949–1959.
[15] D.E. Bornside, C.W. Macosko, L.E. Scriven, Spin coating: one-dimensional model, J. Appl. Phys. 66 (1989) 5185–5193.
[16] R.K. Yonkoski, D.S. Soane, Modeling for spin coating in microelectronic applications, J. Appl. Phys. 72 (1992) 725–740.
[17] J.H. Tortai, Modeling of ultra thin resist film structure after spin-coating and post-application bake, Microelectron. Eng. 73–74 (2004) 223–227.
[18] J. Crank, Free and Moving Boundary Problems, Oxford Science Publications, 1988.
[19] R.H. Perry, D.W. Green (Eds.), Perry's Chemical Engineers' Handbook, seventh ed., McGraw-Hill, New York, NY, 1997.
[20] Y. He, L. Ma, S. Huang, Convection heat and mass transfer from a disk, Heat Mass Transfer 41 (2005) 766–772.
[21] A.F. Mills, Heat Transfer, Irwin, Inc., Homewood, IL, 1992.